Received: 3 October 2021 | Accepted: 3 December 2021

DOI: 10.1111/gcb.16043

Global Change Biology WILEY

RESEARCH ARTICLE

Assessment of the importance of increasing temperature and decreasing soil moisture on global ecosystem productivity using solar-induced chlorophyll fluorescence

Chaoya Dang[1] | Zhenfeng Shao[1] | Xiao Huang[2] | Jiaxin Qian[1] | Gui Cheng[1] | Qing Ding[1] | Yewen Fan[1]

[1]State Key Laboratory Information Engineering Survey Mapping and Remote Sensing, Wuhan University, Wuhan, China

[2]Department of Geosciences, University of Arkansas, Fayetteville, Arkansas, USA

Correspondence
Zhenfeng Shao, State Key Laboratory Information Engineering Survey Mapping and Remote Sensing, Wuhan University, Wuhan 430079, China.
Email: shaozhenfeng@whu.edu.cn

Funding information
National Key R&D Program of China, Grant/Award Number: 2018YFB2100501; 03 Special Research and 5G Project of Jiangxi Province in China, Grant/Award Number: 20212ABC03A09; Zhuhai Industry University Research Cooperation Project of China, Grant/Award Number: ZH22017001210098PWC; National Natural Science Foundation of China, Grant/Award Number: 42090012, 41771452 and 41771454

Abstract

The accurate assessment of the global gross primary productivity (GPP) of vegetation is the key to estimating the global carbon cycle. Temperature (Ts) and soil moisture (SM) are essential for vegetation growth. It is acknowledged that the global Ts has shown an increasing trend, yet SM has shown a decreasing trend. However, the importance of SM and Ts changes on the productivity of global ecosystems remains unclear, as SM and Ts are strongly coupled through soil-atmosphere interactions. Using solar-induced chlorophyll fluorescence (SIF) as a proxy for GPP and by decoupling SM and Ts changes, our investigation shows Ts plays a more important role in SIF in 60% of the vegetation areas. Overall, increased Ts promotes SIF by mitigating the resistance from SM's reduction. However, the importance of SM and Ts varies, given different vegetation types. The results show that in the humid zone, the variation of Ts plays a more important role in SIF, but in the arid and semi-arid zones, the variation of SM plays a more important role; in the semi-humid zone, the disparity in the importance of SM and Ts is difficult to unravel. In addition, our results suggest that SIF is very sensitive to aridity gradients in arid and semi-arid ecosystems. By decoupling the intertwined SM-Ts impact on SIF, our study provides essential evidence that benefits future investigation on the factors the influence ecosystem productivity at regional or global scales.

KEYWORDS
decoupling, ecosystem productivity, remote sensing, soil moisture, solar-induced chlorophyll fluorescence, temperature

1 | INTRODUCTION

Under the context of global climate change, temperature (Ts) presents a notable increasing trend (IPCC, 2013), while soil moisture (SM) suggests otherwise, showing a decreasing trend (Albergel et al., 2013; Deng et al., 2020) with heightened groundwater vulnerability (Nistor, 2019). Suitable Ts and sufficient SM are the basic conditions for vegetation growth. Low SM and high Ts are the two major factors that cause water and heat stress on vegetation, leading to severe damage to agricultural productivity (Madadgar et al., 2017; Shao et al., 2020), and tree mortality (Craig et al., 2010; Park et al., 2012). Studies have shown that SM played an important role in carbon sinks in terrestrial ecosystems (e.g., Green et al., 2019), and studies have also shown that elevated Ts increased vegetation photosynthesis (e.g., Nemani, 2003). Therefore, an in-depth understanding of the impacts of Ts and SM changes on ecosystem productivity is beneficial to the improvement of assessing terrestrial vegetation gross primary productivity (GPP), carbon budget, and climate change.

Numerous studies have been made to assess and predict SM and Ts changes in vegetation productivity and carbon uptake. On the one hand, adequate SM is an essential condition for vegetation growth (Padilla & Pugnaire, 2007). Thus, low SM can directly indicate that vegetation is under water stress. In addition, SM can also capture the effects of water stress on vegetation productivity (Liu et al., 2018; Stocker et al., 2018) and drive plant activity to feedback to the climate (Koster, 2004; Seneviratne et al., 2010) or directly with the climate (Taylor et al., 2012). On the other hand, most of the knowledge on vegetation photosynthesis responses to warming comes from the leaf scale (Niu et al., 2008), where photosynthesis increases with Ts until the optimum Ts is reached, but beyond the optimum Ts, leaf photosynthesis declines in a rapid manner (Medlyn et al., 2002). However, studies have shown that the optimum Ts for ecosystems differ from the leaf scale (Christopher et al., 1995). Elevated Ts usually results in a high vapor pressure deficit (VPD), leading to vegetation stomata that reduce water loss (Williams et al., 2012), which in return might limit vegetation photosynthesis. Recent studies have shown that SM plays an important role in vegetation productivity (Liu, Gudmundsson, et al., 2020; Xu et al., 2019). Also, it has been shown that Ts greatly contributes to vegetation productivity (Huang et al., 2019; Nemani, 2003; Zhang & Shao, 2021). Despite these efforts, the relative importance of elevated Ts and reduced SM in contributing to global ecosystem productivity remains unclear. As SM and Ts are strongly coupled (Seneviratne et al., 2010), whether such coupling effect can lead to an offset between increased Ts and decreased SM on ecosystem productivity deserves investigation. Studies have shown that the Ts usually fails to reach its optimum value in ecosystems (Huang et al., 2019), and an increasing Ts boosts photosynthesis. However, SM is currently showing a decreasing trend (Deng et al., 2020) and decreasing SM can limit photosynthesis (Rogers et al., 2017). Therefore, better knowledge of global ecosystem productivity is much needed under the context of increased Ts coupled with decreased SM.

With the development of satellite observations, new satellite remote sensing products, such as solar-induced chlorophyll fluorescence (SIF), have been widely used. Studies have shown that SIF is sensitive to both water and heat stresses (Sun et al., 2015; Wang et al., 2019; Yoshida et al., 2015). In addition, SIF is a byproduct of vegetation photosynthesis and is homologous to vegetation photosynthetic carbon sequestration. Thus, it is closely related to vegetation GPP (Guanter et al., 2014; Porcar-Castell et al., 2014). SIF also has a near-linear relationship with ecosystem GPP at the ecosystem scale (Frankenberg et al., 2011; Li et al., 2018) and a strong correlation with GPP at flux sites (Chen et al., 2019; Li & Xiao, 2019a). Moreover, high accuracy was obtained for global GPP mapping using SIF (Li & Xiao, 2019b). In this study, we use SIF to represent GPP metrics, taking advantage of evaluating terrestrial photosynthesis and ecosystem function.

We hypothesize that if SM plays a dominating role in ecosystem productivity, high SM is likely to promote ecosystem productivity regardless of changes in Ts. On the contrary, if Ts plays a dominating role in ecosystem productivity, Ts is likely to promote ecosystem productivity regardless of changes in SM. The specific objectives of this study are: (1) to decouple the respective effects of Ts and SM changes on SIF by unraveling the correlations between SM and Ts; (2) to explore the response of SIF of different vegetation types to changes in Ts and SM; (3) to explore the influence of aridity gradients on SIF.

2 | MATERIALS AND METHODS

2.1 | Datasets

In this study, various data products were used to explore the response of global vegetation productivity to decreasing SM and increasing Ts. For consistency, the spatial resolution of these datasets was unified to 0.5° using the mean value method.

2.1.1 | Solar-induced chlorophyll fluorescence (SIF)

Studies have proved that the SIF product from OCO-2 (Orbiting Carbon Observatory-2) has a great potential in estimating GPP (Li et al., 2018). However, given the spatial and temporal sparsity of the data due to the OCO-2 sampling strategy, this data could not be directly used for global-scale analyses. Therefore, we used the spatially continuous global OCO-2 SIF dataset (GOSIF, hereafter SIF) with high spatial and temporal resolution from discrete OCO-2 SIF, MODIS products, and meteorological reanalysis data (Li & Xiao, 2019a) (http://data.globalecology.unh.edu/data/GOSIF_v2/). SIF was available from 2000 to 2020 with a spatial resolution of 0.05° ×0.05° and a temporal resolution of 8-day, monthly, and yearly. Despite that GOSIF is a great proxy for SIF and SIF is a great proxy for photosynthesis, we acknowledge that they are not perfect proxies.

The monthly mean SIF data from GOME-2 (Global Ozone Monitoring Experiment-2) covers February 2007 to March 2019 (Level 3, v28, https://avdc.gsfc.nasa.gov/pub/data/satellite/MetOp/GOME_F/) with a spatial resolution of 0.5° ×0.5°. It was derived from the inversion of the far-infrared spectrum peak at 740 nm with an improved algorithm (Joiner et al., 2013; Köhler et al., 2014). This SIF product has been quality controlled to exclude heavy cloud effects and to synthesize monthly averages (Sun et al., 2015), but data missing problems still exist.

2.1.2 | Gross primary productivity (GPP)

Derived from the Global Land Surface Satellite (GLASS) GPP product (Liang et al., 2020), the GPP products span from 2000 to 2018 with a spatial resolution of 0.05° and 8-day, monthly, and yearly temporal resolutions (http://www.glass.umd.edu/Download.html). We used the GPP products from GLASS to further validate the spatiotemporal consistency between SIF and GPP.

2.1.3 | Soil moisture (SM)

SM data were derived from the Global Land Evaporation Amsterdam Model (GLEAM) v3.5a surface SM and root SM (SM_{root}) (https://www.gleam.eu). The GLEAM surface SM was generated by assimilating the data from European Space Agency's Climate Change Initiative (ESA CCI) SM (v5.3) using surface model GLEAM (Burgin et al., 2017; Martens et al., 2017; Miralles et al., 2011) through an optimized Newtonian light extrapolation method (Martens et al., 2015). The overall performance accuracy of GLEAM SM products is considerably high (median $R = 0.71$; Beck et al., 2021). The GLEAM SM products span from 1980 to 2020 with a spatial resolution of 0.25° × 0.25° and daily, monthly, and yearly temporal resolutions. Moreover, the data gaps have been filled relative to ESA CCI SM data, leading to better spatial coverage on the whole terrestrial ecosystem.

2.1.4 | Temperature (Ts)

Monthly mean near-surface temperature data from 1901 to 2020 were obtained from the Climatic Research Units Time series (CRU Ts) v4.05 product (Harris et al., 2020) (https://crudata.uea.ac.uk/cru/data/hrg/), with a spatial resolution of 0.5° × 0.5°.

2.1.5 | Aridity index (AI)

The aridity index (AI) was defined as the ratio of precipitation to potential evapotranspiration. Precipitation data from CRU Ts v4.05 (Harris et al., 2020) and potential evapotranspiration data from GLEAM v3.5a (Martens et al., 2017) from 2000 to 2020 were used in this study. Following a widely used protocol (Feng & Fu, 2013; Yao et al., 2020), drylands were defined as areas with an AI less than 0.65; subtypes of aridity were defined by AI ranges: hyperarid (AI ≤ 0.05), arid (0.05 < AI ≤ 0.2), semi-arid (0.2 < AI ≤0.5), and semi-humid semi-arid (0.5 < AI < 0.65) and humid (AI ≥ 0.65).

2.1.6 | Vegetation type

The vegetation cover types were derived from the MODIS MCD12C1 land cover type product with the International Geosphere-Biosphere Programme (IGBP) classification scheme (https://search.earthdata.nasa.gov/). MODIS IGBP land cover data are an annual synthetic product with a spatial resolution of 0.05°. The vegetation area was derived based on MODIS land cover types, using the vegetation cover proportion aggregated to a spatial resolution of 0.5°, where areas with vegetation cover proportion ≥75% were defined as vegetation; otherwise, they were defined as non-vegetation. Each pixel that covers 0.5° by 0.5° contains a certain vegetation-type label.

2.2 | Methods

The technical flowchart that describes the main ideas of this study, including data collection, pre-processing, indicators calculation, methods, and analysis conclusions, is present in Figure 1. The decoupling method and analysis for SM-Ts are the core components of this study. We verified the reliability of our results by comparing them with results from other methods and data sources.

2.2.1 | Standardized anomaly

In order to explore the impacts of changes in Ts and SM on SIF under global climate change, pixel-wise standardized anomalies of the above indicators were calculated. The standardized anomalies were calculated as deviations from multi-year averages, normalized using standard deviations from 2000 to 2020. The calculation of the standardized anomaly follows (Liu et al., 2021; Wang et al., 2019):

$$SA(i,j,t) = \frac{X(i,j,t) - \overline{X}(i,j,m)}{SD(i,j,m)} \quad (1)$$

where $SA(i, j, t)$ is the standardized anomaly of pixel (i, j) at time t; $X(i, j, t)$ is the original values of the pixel (i, j) at time t; $\overline{X}(i, j, m)$ is the mean value of pixel (i, j) in the mth month of each year from 2000 to 2020; $SD(i, j, m)$ is the standard deviation of pixel (i, j) in the mth month of each year from 2000 to 2020. The m, ranging from 1 to 12, denotes the mth month of the year.

2.2.2 | Binning

The impact of Ts and SM on SIF was decoupled utilizing bins, as Liu, Gudmundsson, et al. (2020) showed that binning could decouple the two variables to a large extent. Based on the standardized anomaly data, we determined segmentation thresholds for each pixel of SA_{SM} and SA_{Ts}, which were applied to bins of the data. The data of all variables were divided into eight bins, i.e., [−2.–1.5), [−1.5.–1), [−1.–0.5), [−0.5.–0), [0.0.5), [0.5.1), [1.1.5), and [1.5.2], depending on SA_{Ts} or SA_{SM}. Next, within each SA_{Ts} bin (i = 1, 2,..., 8), the ranking from minimum $\Phi_{i,min}$ to maximum $\Phi_{i,max}$ was determined based on the ith SA_{Ts} bin and the threshold value. Similarly, in each SA_{SM} bin (j = 1, 2,..., 8), the ranking from minimum $\theta_{j,min}$ to maximum $\theta_{j,max}$ ranking was determined by the jth SA_{SM} bin and the threshold value. Data were eliminated if they were less than 10 in each bin.

The mean values of bins were used to quantify the effect of SM and Ts on SIF. Excluding the SM-Ts coupling, the influence of Ts on SIF is denoted as $\triangle SA_{SIF}(SA_{Ts}|SA_{SM})$. In this study, we calculated the difference between the highest SA_{Ts} and the lowest SA_{Ts} corresponding to SA_{SIF} in each SA_{SM} binning ($\triangle SA_{SIF}(SA_{Ts}|SA_{SM})$), which was given by (Liu, Gudmundsson, et al., 2020):

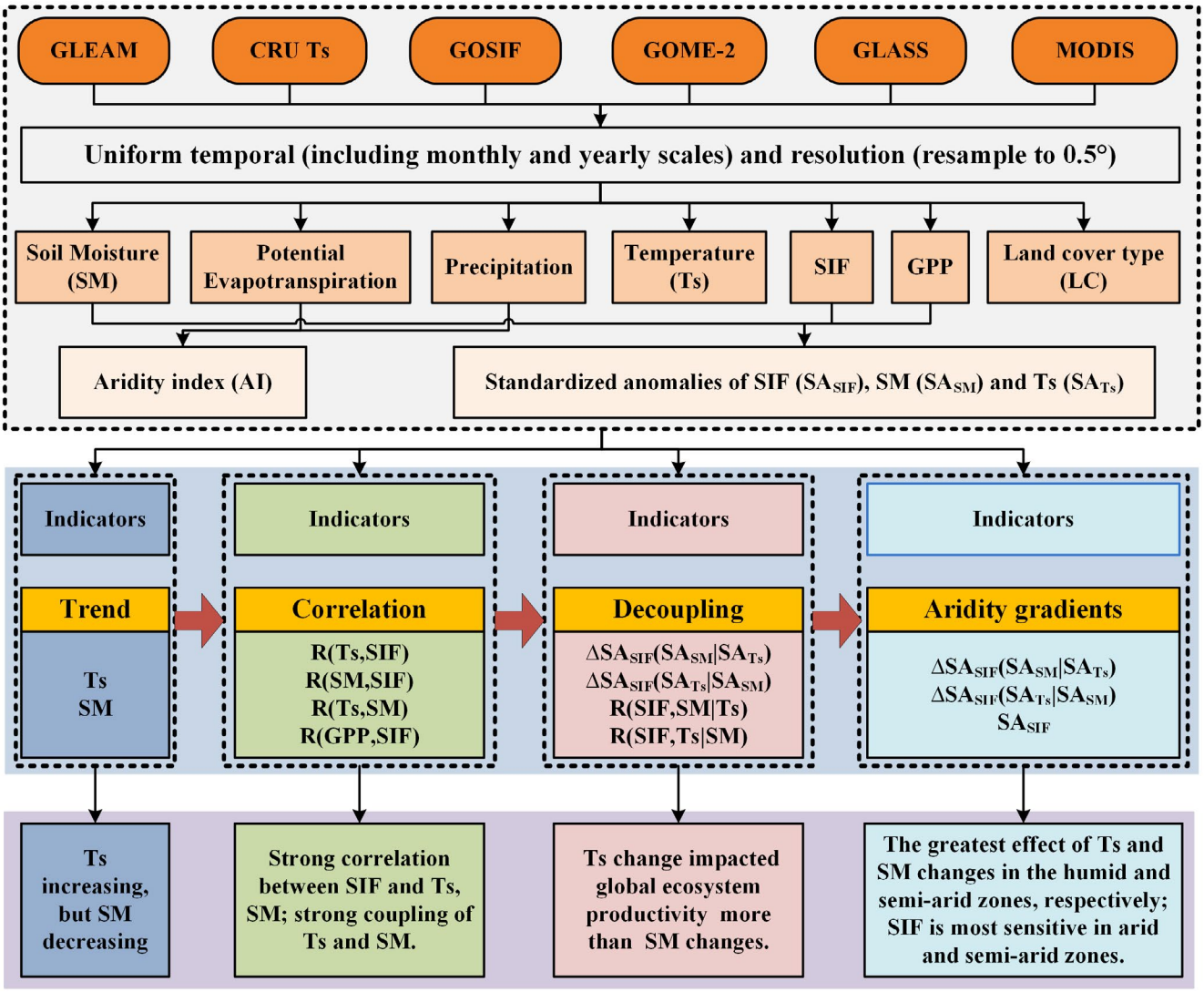

FIGURE 1 The technical flowchart of this study [Colour figure can be viewed at wileyonlinelibrary.com]

$$\Delta SA_{SIF}\left(SA_{Ts}|SA_{SM}\right) = \frac{1}{I} \times \sum_{i=1}^{I}\left(SA_{SIFi,\phi_{i,max}} - SA_{SIFi,\phi_{i,min}}\right) \quad (2)$$

where I is the total number of bins SA_{Ts}; i is the index number of the ith SA_{Ts} bins; $\Phi_{i,min}$ and $\Phi_{i,max}$ are the sequential numbers corresponding to the minimum and maximum of SA_{Ts} in the ith SA_{SM} bin.

Similarly, excluding the SM-Ts coupling, the influence of SM on SIF is denoted as $\Delta SA_{SIF}\left(SA_{SM}|SA_{Ts}\right)$, which stemmed from the variation of high SA_{SM} to low SA_{SM} on SA_{SIF} in each SA_{Ts} bin. The calculation follows Liu, Gudmundsson, et al. (2020):

$$\Delta SA_{SIF}\left(SA_{SM}|SA_{Ts}\right) = \frac{1}{J} \times \sum_{j=1}^{J}\left(SA_{SIFj,\theta_{j,max}} - SA_{SIFj,\theta_{j,min}}\right) \quad (3)$$

where J is the total number of bins SA_{SM}; j is the label of the jth SA_{SM} bin; $\theta_{j,min}$ and $\theta_{j,max}$ are the sequential numbers of the jth SA_{Ts} bin corresponding to the smallest and largest SA_{SM}. Studies have shown that the responses of plant photosynthesis to SM and Ts can be non-linear (Green et al., 2019; Sage & Kubien, 2007), and our approach is able to capture such non-linearity.

2.2.3 | Partial correlation coefficient

To better understand the independent effects of Ts and SM on SIF, we adopted the partial correlation method at the pixel level to analyze the correlation between Ts and SIF (referred to as R (Ts, SIF|SM)), excluding the influence of SM. Similarly, we also analyzed the correlation between SM and SIF (called R (SM, SIF|Ts)), excluding the impact of Ts. The partial correlation formula was:

$$R_{(1,2|3)} = \frac{R_{12} - R_{13} \times R_{23}}{\sqrt{1 - R_{13}^2} \times \sqrt{1 - R_{23}^2}} \quad (4)$$

where $R_{(1,2|3)}$ is the partial correlation coefficient between variable 1 and variable 2 after controlling for the linear effect of variable 3; R_{12},

R_{13}, and R_{23} are correlation coefficients between variable 1 and variable 2, variable 1 and variable 3, and variable 2 and variable 3, respectively.

3 | RESULTS AND DISCUSSION

3.1 | Spatial and temporal trends of global Ts, SM, and SIF

Many pieces of evidence have suggested an increasing trend of global Ts. Our results suggest that the increases in Ts were heterogeneous from spatial and temporal perspectives (Figure 2a, Figures S1a and S2a). The Ts trends from 1901 to 2020 from the global climate dataset observed by the CRU were analyzed. From Figure S1a, we observed that the Ts dynamics could be divided into two major time periods: the first period, i.e., 1901–1980, showed a slow Ts increase (0.00342°C a^{-1}), and the second period, i.e., 1980–2020, showed an exacerbated increasing rate (0.03123°C a^{-1}), about 10 times of that before 1980. From Fig. 2a, 87.59% of the Ts increase from 2000 to 2020 in the vegetated areas, within which 56.19% of the increase is at the 95% significance level (Figure S2a). The pixel-wise frequency of warming from 2000 to 2020 relative to 1980 to 1999 was concentrated from 60% to 90% (Figure S3a, d).

Similar to Ts, the global trend of SM reduction presents a heterogeneous pattern in time and space (Figure 2b, Figures S1b and S2b). The trend of SM was analyzed using GLEAM assimilated global raster surface SM and root SM from 1980 to 2020. Figure S1b and c demonstrated a decreasing trend of surface SM (−0.00009865 m^3 m^{-3} a^{-1}) and root SM (−0.00007324 m^3 m^{-3} a^{-1}), respectively, which was consistent with the findings of existing studies (Albergel et al., 2013; Deng et al., 2020). Figure 2b revealed that 51.23% of the vegetated areas experienced a decline in SM, and 26.78% of them reached the 95% significance level (Figure S2b). Figure S3b showed that pixel-wise frequency of SM reduction was concentrated between 40% and 70% from 2000 to 2020 relative to 1980 to 1999. In addition, the pixel-wise frequency of Ts increase and SM decrease was focused at 25% to 55% (Figure S3c).

From Figure 2c, 75.60% of the areas presented an increase in SIF, of which 47.41% showed increased SIF at the 95% significance level. Huang et al. (2019) concluded that Ts did not reach the optimum temperature for vegetation photosynthesis. Hence, a higher Ts is expected to further enhance vegetation photosynthesis, leading to an increased SIF. Besides, Liu, Gudmundsson, et al. (2020) stated that SM was positively correlated with SIF. Therefore, a reduction in SM would inhibit vegetation photosynthesis. The global distribution of areas with increased SIF was not fully consistent with the distribution of areas with increased Ts and SM (Figure 2). In particular, inconsistency in SIF changes occurred for areas with increased Ts and decreased SM and areas with decreased Ts and increased SM. Therefore, the independent effect of Ts and SM on the productivity of global ecosystems remains unclear.

3.2 | Coupling of Ts and SM affects ecosystem productivity

The soil-vegetation-atmosphere environments are strongly intertwined with a complicated mechanism. The difficulty in unraveling the respective effects of SM and Ts on ecosystem productivity stemmed from the strong coupling of SM and Ts (Koster et al., 2006; Seneviratne et al., 2010; Sonia et al., 2010). Rising Ts leads to increased evapotranspiration, which in turn leads to further soil drying; decreasing SM results in reduced evapotranspiration, which in turn causes elevated Ts. Because of strong SM-Ts coupling (Figure 3c, e), both high Ts and SM were correlated with high ecosystem GPP indicated by SIF (Figure 3a, b). From Figure 3d, e, we observed that SIF was strongly correlated with GPP at the global scale. The correlation coefficients between Ts and SIF were generally positive at the global

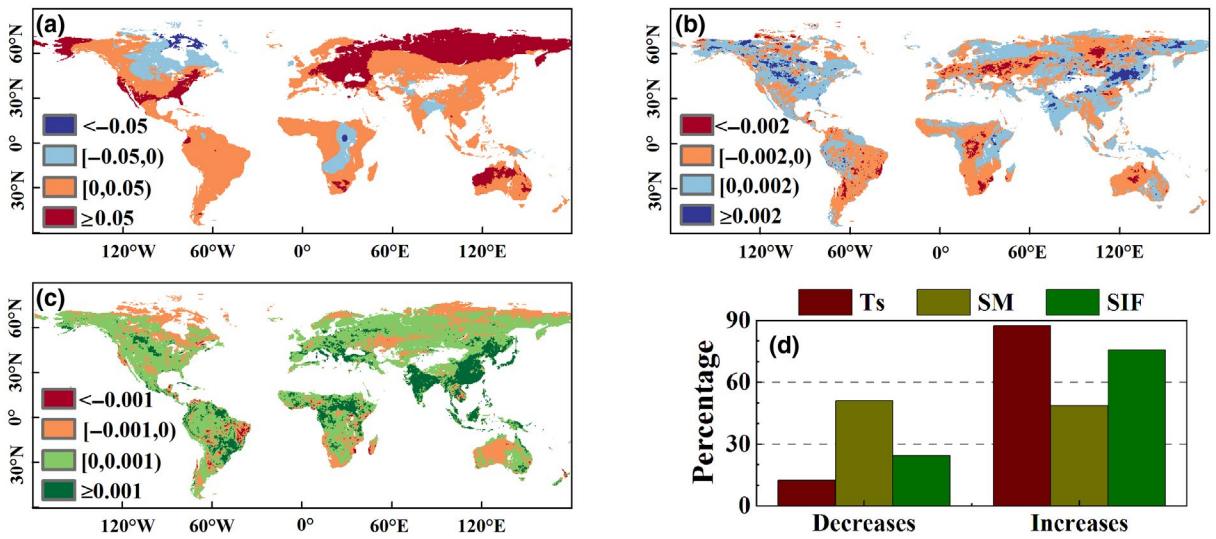

FIGURE 2 The trend of global Ts, SM, and SIF from 2000 to 2020. (a) Ts trend from 2000 to 2020. (b) SM trend from 2000 to 2020. (c) SIF trend from 2001 to 2020. (d) Distribution of relative frequencies (%) of decreases and increases in Ts, SM, and SIF [Colour figure can be viewed at wileyonlinelibrary.com]

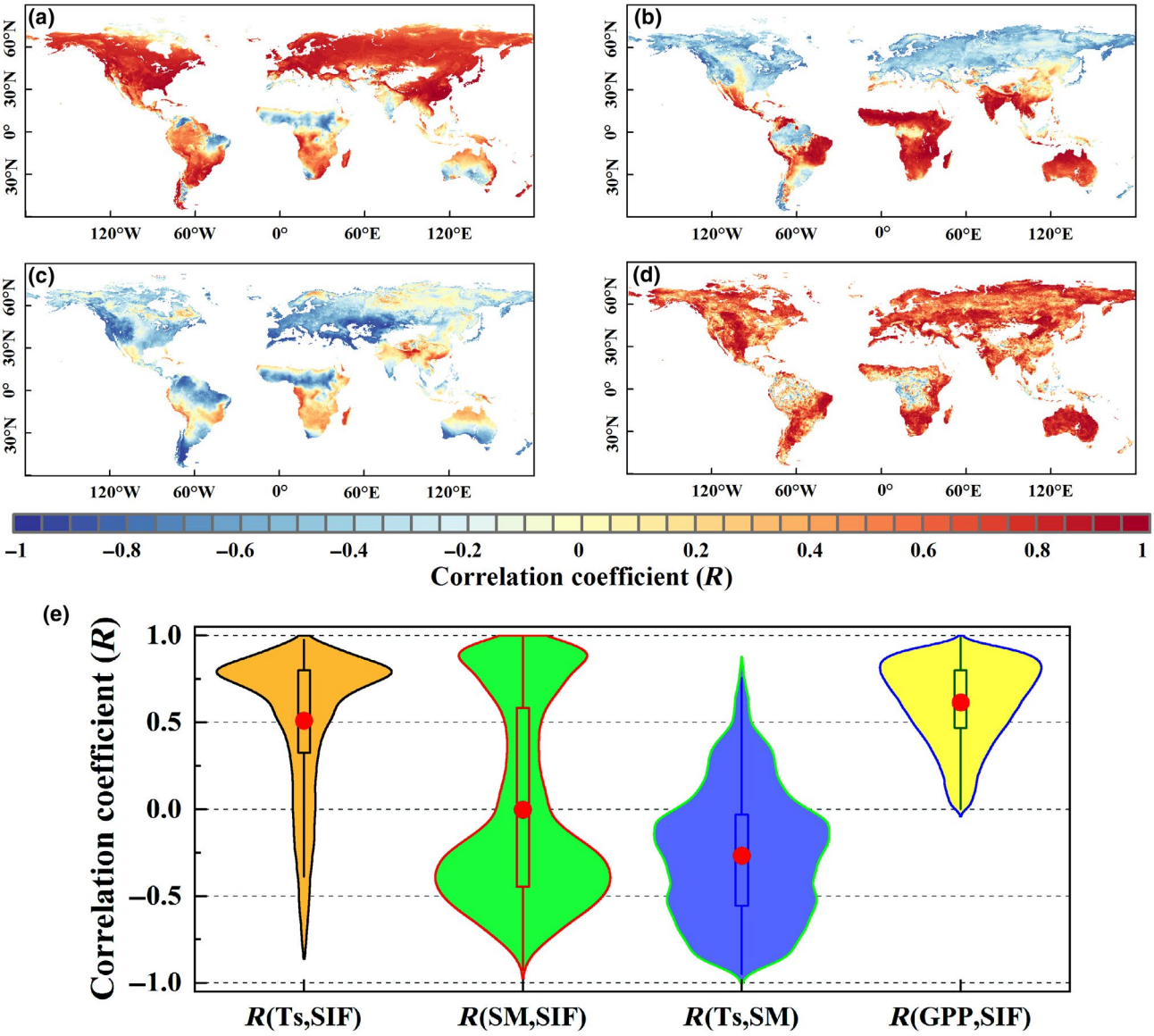

FIGURE 3 The strong coupling of Ts and SM confuses the impact on ecosystem productivity. (a) Spatial distribution of Pearson's correlation coefficients between solar-induced chlorophyll fluorescence and temperature (R(Ts,SIF)). (b) Spatial distribution of Pearson's correlation coefficients between solar-induced chlorophyll fluorescence and soil moisture (R(SM,SIF)). (c) Spatial distribution of Pearson's correlation coefficients between temperature and soil moisture (R(Ts,SM)). (d) Spatial distribution of Pearson's correlation coefficients between solar-induced chlorophyll fluorescence and gross primary productivity (R(GPP,SIF)). (e) Violin plots of correlation coefficients between Ts and SIF, SM and SIF, Ts and SM, and GPP and SIF, respectively. The red dots indicate the median values, the rectangular boxes cover the interquartile range, and thin lines reach the 5th and 95th percentiles. When the correlation coefficient is greater than 0.124 and 0.126 or less than −0.124 and −0.126, it reaches the 95% and 99% significance level, respectively [Colour figure can be viewed at wileyonlinelibrary.com]

scale (Figure 2e) but were negative near the equator and in southern Australia (Figure 3a). The correlations between SM and SIF were positive at low latitudes and southern hemisphere (except tropical rainforests) but negative at middle and high latitudes in the northern hemisphere (Figure 3b, e). Given the strong SM-Ts coupling, in regions with high SM and high Ts, the correlation between SM and SIF might be a byproduct of the correlation between Ts and SIF and vice versa. In regions with high Ts but low SM, the correlation directions between Ts and SIF were not consistent. Thus, the correlation between SM and Ts constituted an often-overlooked confounding factor when assessing the role of SM and Ts on ecosystem productivity. In the tropics, correlations between SIF and SM or SIF and Ts remained weak, indicating the possible influence of CO_2 concentration, nitrogen deposition or radiation effects, which need to be further explored.

3.3 | Decoupling the impacts of Ts and SM on SIF

There existed a strong negative correlation between SM and Ts, evidenced by the observations that low SM was always accompanied by high Ts (Figure 3c, e), which was consistent with previous

studies (Koster et al., 2006; Seneviratne & Stöckli, 2007; Sonia et al., 2010). Liu, Gudmundsson, et al. (2020) revealed that the interaction between SM and VPD could be well decoupled with a binning approach. Therefore, we decoupled SM-Ts from −2 to 2 (95.45% of the total data) at intervals of 0.5 to 8 bins based on standardized anomaly data of SM or Ts. The analytical hypothesis of this study was that if SM dominated ecosystem productivity, high SM would promote ecosystem productivity regardless of changes in Ts, and if Ts played a dominant role in ecosystem productivity, then high Ts would promote ecosystem productivity independent of changes in SM.

To further validate the above hypothesis, we utilized global vegetation averages for illustration. Without decoupling SM-Ts, it was difficult to determine whether the increase in SIF was caused by high SM, high Ts, or a combination of both. When observing the change in SA_{SIF} on the SA_{Ts} gradient in the SA_{SM} bin (without SM-Ts coupling), high SA_{Ts} led to increased SA_{SIF}, but SA_{SIF} remained unchanged in the high SA_{SM} case (Figure 4a). In addition, high SA_{SM} also resulted in an increase of SA_{SIF} in the SA_{Ts} bin, but high SA_{SM} decreased SA_{SIF} in the high SA_{Ts} sub-box (Figure 4b). The above results indicated that both high SA_{Ts} and high SA_{SM} could increase SA_{SIF} for conditions without SM-Ts coupling at the global scale. In other words, the notably increased SA_{SIF} suggested that neither SA_{Ts} nor SA_{SM} was a byproduct of SM-Ts coupling. The respective impact of SA_{SM} and SA_{Ts} on SA_{SIF} was also shown in Figure 4c. Without SM-Ts coupling, changes in SA_{SIF} from low SA_{Ts} to high SA_{Ts} (called $\triangle SA_{SIF}(SA_{Ts}|SA_{SM})$) could quantify the magnitude of SA_{Ts}'s effect on SA_{SIF}. Likewise, without SM-Ts coupling, changes in SA_{SIF} from low SA_{SM} to high SA_{SM} (called $\triangle SA_{SIF}(SA_{SM}|SA_{Ts})$) could quantify the extent of the effect of SA_{SM} on SA_{SIF}. In this study, the effects of SM and Ts on SIF were evaluated via two methods, (1) using the SA_{SIF} in the largest SA_{SM} interval minus the SA_{SIF} in the smallest SA_{SM} bins or the SA_{SIF} in the highest SA_{Ts} interval minus the SA_{SIF} in the lowest SA_{Ts} bins, and (2) using the partial correlation coefficient to analyze the effect of SM (called R (SIF, SM|Ts)) or Ts (R (SIF, Ts|SM)) on the magnitude of the SIF. From Figure 4c, Ts ($\triangle SA_{SIF}(SA_{Ts}|SA_{SM}) = 0.8164$) has a stronger correlation with $\triangle SA_{SIF}$ compared with SM ($\triangle SA_{SIF}(SA_{SM}|SA_{Ts}) = 0.4587$). Therefore, the comparison of $\triangle SA_{SIF}$ $(SA_{Ts}|SA_{SM})$ and $\triangle SA_{SIF}$ $(SA_{SM}|SA_{Ts})$ could determine the importance of the respective

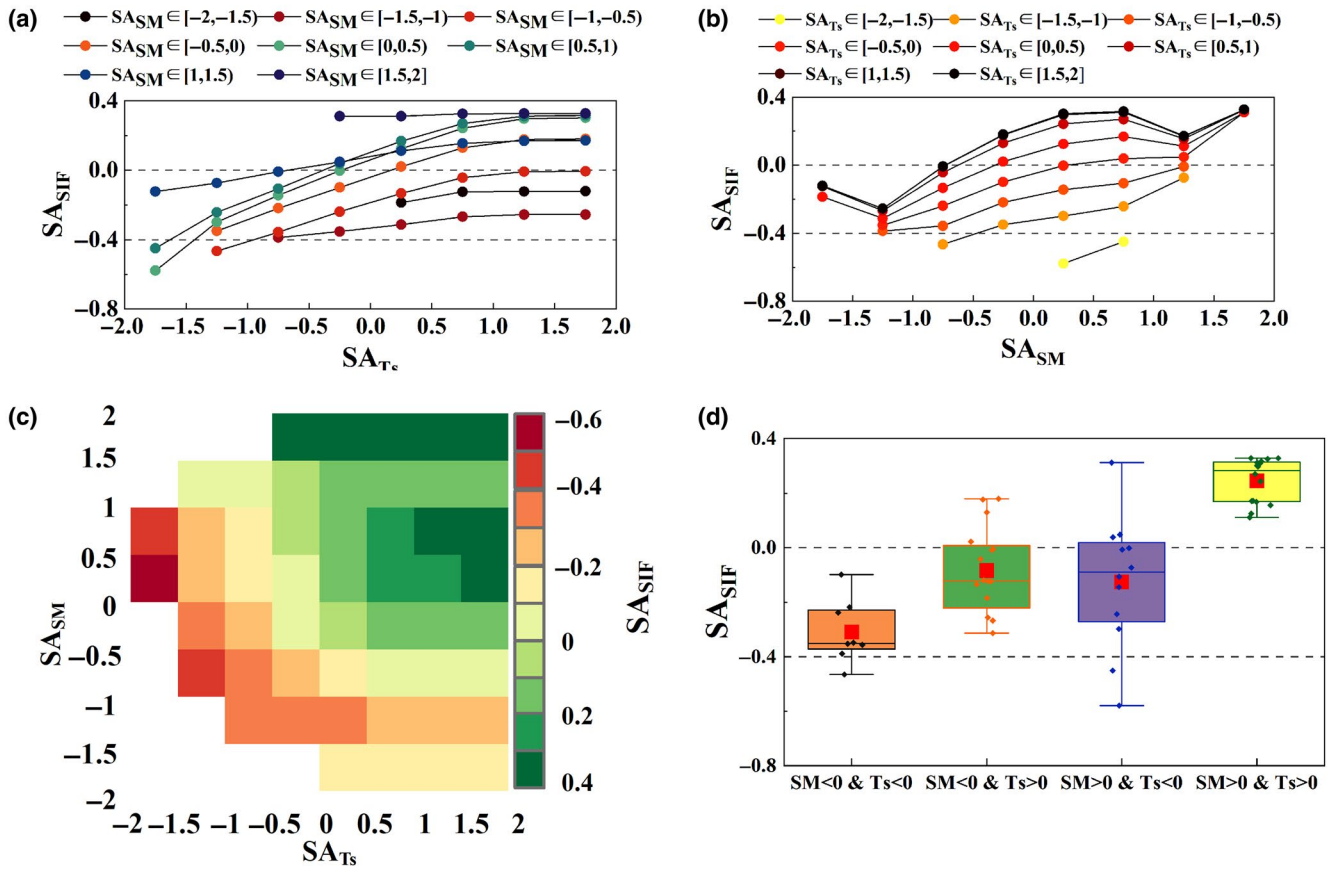

FIGURE 4 Decoupling the effects of Ts and SM on ecosystem productivity. (a) Monthly standardized anomalies of SIF and Ts, binned by SM standardized anomalies; circles indicate mean SIF standardized anomalies within each bin of SM standardized anomalies. (b) Monthly standardized anomalies of SIF and SM, binned by Ts standardized anomalies; circles denote mean SIF standardized anomalies within each bin of Ts standardized anomalies. (c) the mean SIF standardized anomalies in each bin of standardized anomalies of Ts and SM; horizontal numbers represent the Ts influence on SIF without Ts-SM coupling ($\triangle SA_{SIF}(SA_{Ts}|SA_{SM})$); vertical numbers represent the SM influence on SIF without Ts-SM coupling ($\triangle SA_{SIF}$ $(SA_{SM}|SA_{Ts})$). (d) standardized anomalies of Ts and SM under different conditions of SIF standardized anomaly box plot distributions; circles indicate SIF standardized anomalies values for each condition; red squares indicate the corresponding mean [Colour figure can be viewed at wileyonlinelibrary.com]

factors in the SM-Ts coupling. In addition, the partial correlation coefficient based on the mean of global variables showed that Ts ((SIF, Ts|SM) = 0.759, $p < .001$) was more strongly correlated with SIF than SM (R(SIF,SM|Ts) = 0.418, $p = .075$). Thus, the results from both methods were consistent, indicating a stronger role of Ts in terms of promoting global ecosystem productivity than SM. Moreover, Figure 4d revealed that when both SA_{SM} and SA_{Ts} were less than 0, the mean value of SA_{SIF} was −0.309; when $SA_{SM} < 0$ but $SA_{Ts} > 0$, the mean value of SA_{SIF} was −0.083; when $SA_{SM} > 0$ but $SA_{Ts} < 0$, the mean value of SA_{SIF} was −0.126, and when both SA_{SM} and SA_{Ts} is greater than 0, the mean value of SA_{SIF} became 0.245. Thus, high SA_{SM} and high SA_{Ts} could jointly promote ecosystem productivity, but SA_{Ts} enhanced it in a stronger manner than SA_{SM}.

Although the increase in Ts promoted vegetation productivity more than SM at the global scale, the large variation in root depth across vegetation types (e.g., forests and grasslands) might underestimate the impact of SM (only considering relatively superficial SM). However, deep SM could also be associated with deep-rooted vegetation growth (Humphrey et al., 2018). Thus, we further explored the degree of influence of Ts and SM on different vegetation types. Without SM-Ts coupling, evergreen broadleaf forest (Figure S4), mixed forest (Figure S5), and woody savannas (Figure S7) failed to promote SA_{SIF} from low SA_{SM} to high SA_{SM}, but showed a remarkable promotion of SA_{SIF} from low SA_{Ts} to high SA_{Ts}; where the SA_{SM} of either binning had a trivial increase in SA_{SIF} at high SA_{Ts}. In the lack of SM-Ts coupling, SA_{SIF} increased in savanna (Figure S8) from low SA_{SM} or SA_{Ts} to high SA_{SM} or SA_{Ts}, but SA_{Ts} promoted SA_{SIF} increase less than evergreen broadleaf forest, mixed forest, and woody savannas, and SA_{SM} led to a slightly increasing trend of SA_{SIF}. In the absence of SM-Ts coupling, open shrublands (Figure S6), grassland (Figure S9), and crops (Figure S10) showed a greater contribution to SA_{SIF} increase from low SA_{SM} to high SA_{SM} than SA_{Ts}. Without SM-Ts coupling, low vegetation cover in (Figure S11) displayed a clear tendency to promote SA_{SIF} increase from low SA_{SM} to high SA_{SM}, and only a slight trend to increase SA_{SIF} from low to high SA_{Ts} in high SA_{SM} conditions. Thus, there were differences in response to Ts and SM for vegetation types with different root depths. Regions with a lower proportion of trees were more sensitive to SM response at the global scale, which was consistent with previous findings (Walther et al., 2019) and could further confirm the validity of the results in this study. In comparison, areas with higher proportions of trees were more sensitive to the response of Ts at the global scale. Thus, the results revealed the disparity in dominant factors of productivity among vegetation types, providing essential evidence that benefits future investigation on the factors the influence ecosystem productivity at regional or global scales.

Next, we explored the global effects of the individual SM and Ts on the SIF at the pixel level. To ensure spatial comparability, the SIF was standardized anomalies at the pixel level, taking values within plus and minus two standard deviations, respectively. As shown in Figure 5a, b, positive values of $\triangle SA_{SIF}$ ($SA_{Ts}|SA_{SM}$) accounted for 84.80% of the global vegetation cover, suggesting that high SA_{Ts} played a strong role in promoting SA_{SIF}. Moreover, the increase in ecosystem productivity at high latitudes was mainly influenced by elevated Ts, consistent with the findings of Liu, Wennberg, et al. (2020). However, the proportion of $\triangle SA_{SIF}$ ($SA_{Ts}|SA_{SM}$) less than 0 accounted for only 15.20%, which was mainly distributed near the equator and in tropical and subtropical regions at low latitudes (southern North America, South America, Africa, and southwestern Asia and Australia). From Figure 5c, d, the percentage of positive $\Delta SA_{SIF}(SA_{SM}|SA_{Ts})$ was 64.08%, also indicating that high SA_{SM} promoted SA_{SIF}, which was consistent with our understanding of vegetation physiology and the findings of previous studies (Seneviratne & Stöckli, 2007; Stocker et al., 2018). ΔSA_{SIF} ($SA_{SM}|SA_{Ts}$) was found to be negative at high latitudes, i.e., northern South America and central Africa. At high latitudes, elevated Ts promoted vegetation productivity, but high SM limited vegetation productivity (Figure 5a, c). In the tropics and subtropics near the equator, increased Ts led to reduced vegetation productivity (Figure 5a), and the productivity of high trees might not respond to surface SM precisely so that forests with increased SM have seen declined productivity. In addition, we obtained similar spatial distributions using GOME-2 SIF data with a decoupling method to analyze the effects of Ts and SM on productivity (Figure S12). Moreover, decoupling Ts-SM_{root} revealed that the impact of Ts and SM_{root} on ecosystem productivity is highly consistent with Ts and surface SM (Figure 5 and Figure S15). Globally, changes from the lowest SA_{Ts} to the highest SA_{Ts} under a constant SA_{SM} improved SA_{SIF} by 26.50% on average. However, changes from the driest to the wettest SA_{SM} for constant SA_{Ts} raised SA_{SIF} by 16.52% on average. The effect of SA_{Ts} on SA_{SIF} at the pixel level over SA_{SM} was mainly concentrated in the middle and high latitude regions (Figure 5e, f). SA_{SM} was more important than SA_{Ts} in 40.18% of the globe, which was mainly distributed in the middle and low latitudes (Figure 5e, f). If changes in Ts and SM own the same magnitude of impact on terrestrial ecosystem productivity, when $SA_{Ts} + SA_{SM} = 0$, SA_{SIF} is expected to be 0. Thus, the pixel with $SA_{Ts} + SA_{SM} < 0.001$ (indicating the same magnitude of Ts and SM changes) was filtered globally. When $SA_{Ts} < 0$ (or $SA_{Ts} > 0$), i.e., $SASIF = -0.01805 < 0$ (or $SA_{SIF} = 0.00221 > 0$), it indicates that the effect of Ts changes on ecosystem productivity is greater than that of SM changes. However, Humphrey et al. (2021) revealed that soil moisture-atmosphere feedback could dominate the changes in carbon uptake in terrestrial ecosystems, where SM changes play a major role in influencing global land carbon uptake variability. Two main reasons are behind the discrepancy from our study and Humphrey et al. (2021): first, different indicators were analyzed. In this study, we analyzed terrestrial ecosystem productivity (i.e., GPP), while Humphrey et al. (2021) analyzed terrestrial ecosystem carbon uptake (i.e., Net biome productivity, NEP, where NEP equals GPP minus autotrophic respiration, heterotic respiration, and photosynthetic products consumed by natural and anthropogenic disturbances). Second, different analytical methods were employed. We used the decoupling method to study the magnitude of the contribution of temperature and soil moisture changes to GPP changes, respectively, while Humphrey et al. (2021) considered the extent of soil moisture-atmosphere feedback effects on NEP changes.

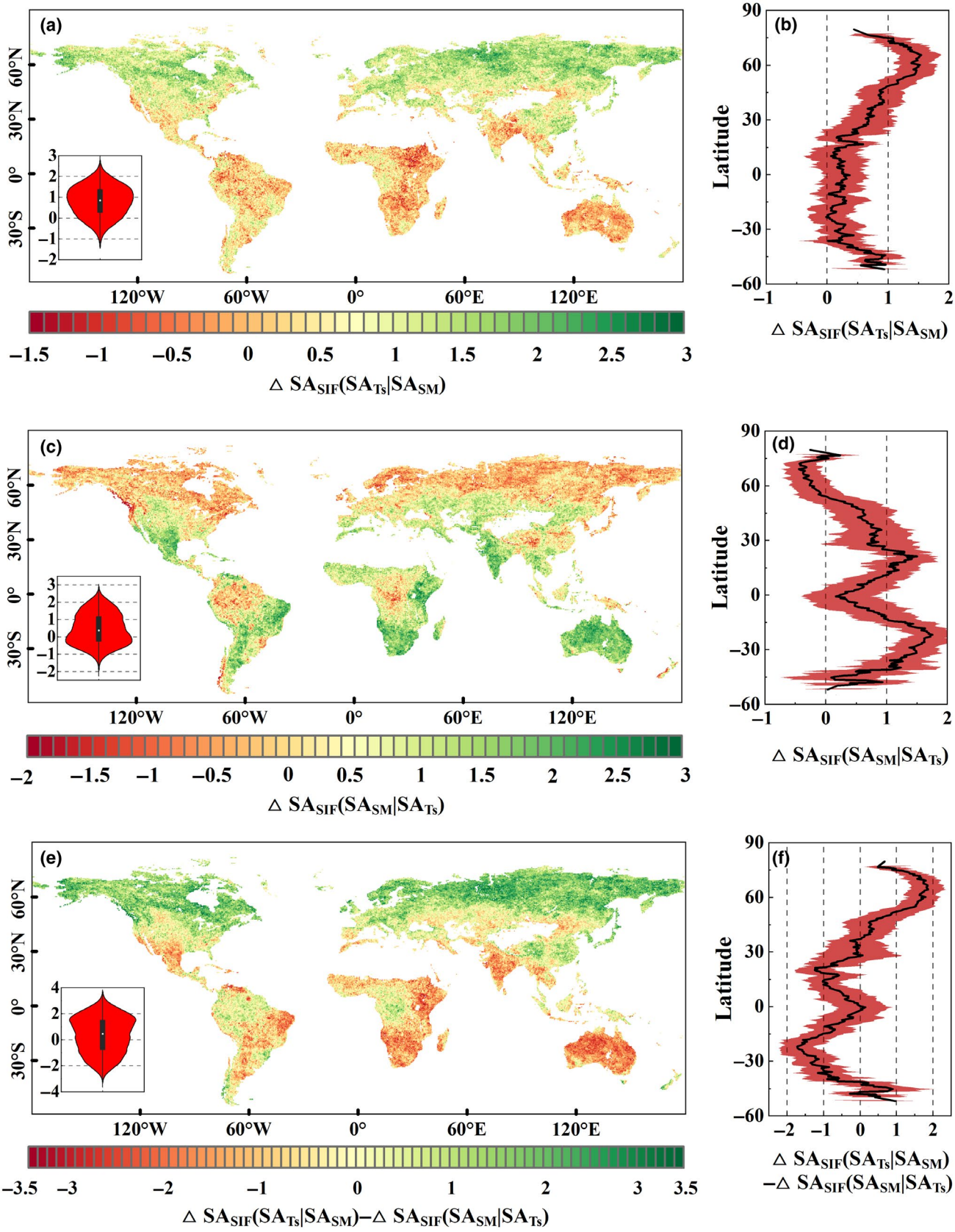

FIGURE 5 Global impacts of Ts and SM on ecosystems production. (a, c, and e) indicate that the spatial distribution of SIF changes due to high Ts ($\triangle SA_{SIF}$ ($SA_{Ts}|SA_{SM}$)), high SM ($\triangle SA_{SIF}$ ($SA_{SM}|SA_{Ts}$)), and their absolute differences ($\triangle SA_{SIF}$ ($SA_{Ts}|SA_{SM}$) − $\triangle SA_{SIF}$ ($SA_{SM}|SA_{Ts}$)), respectively. (b, d, and f) reveal the mean values of Ts and SM influence on SIF and their differences in absolute values. The black line indicates the mean, and the red shaded bands indicate the standard deviation [Colour figure can be viewed at wileyonlinelibrary.com]

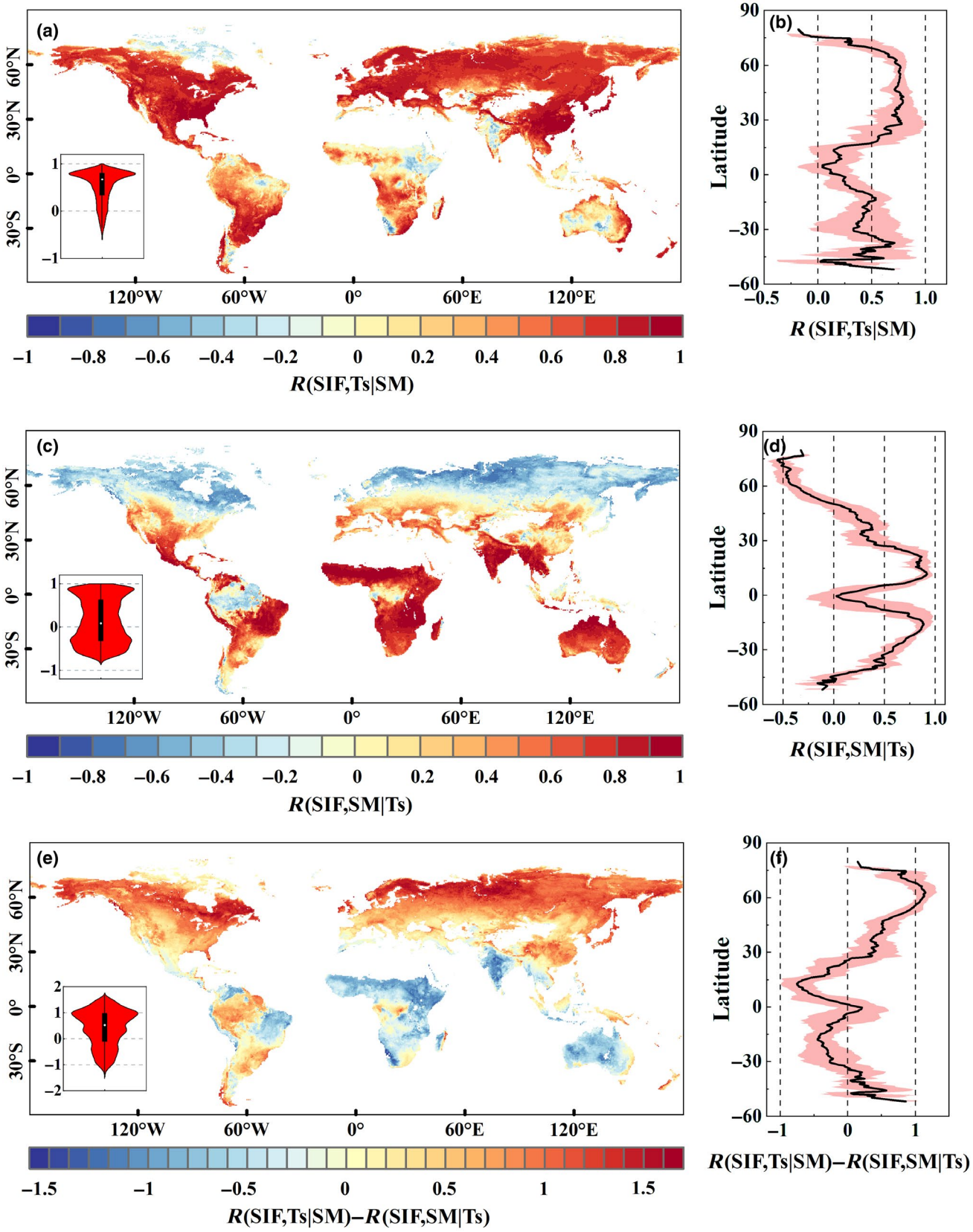

FIGURE 6 Global spatial patterns correlations between SIF with Ts and SM. (a, c, and e) reveal the partial correlation coefficients of SIF with Ts (R(SIF, Ts|SM), (SM is the control variable)), SM (R(SIF,SM|Ts), (Ts is the control variable)), and their absolute differences (R(SIF, Ts|SM) - R(SIF,SM|Ts)) at monthly basis from 2000 to 2020. (b, d, and f) reveal the mean values of the partial correlation coefficients between SIF and Ts, SM, and their differences in absolute values. The black line indicates the mean value, and the pink shaded band indicates the standard deviation [Colour figure can be viewed at wileyonlinelibrary.com]

In addition, partial correlation analysis showed that SIF was significantly correlated with Ts when excluding the effect of SM (Figure 6a, b). As shown in Table 1, 89.70% (87.56% ($p < .05$)) of the valid vegetation areas were positively correlated. Negative correlations (10.30% ($p < .05$)) were found in northeastern North America, India, northeastern Africa, and parts of southwestern Australia (Table 1 and Figure S14a, c). From Figure 6c, d, the proportion of positive partial correlations (excluding the effect of Ts) between SIF and SM was 54.23% (51.68% ($p < .05$)) (Table 1 and Figure S14a, c). However, areas where the negative correlation accounts for 45.77% ($p < .05$) of the global vegetation were mainly distributed in the middle and high latitudes and northwest South America (Table 1 and Figure S14a, c). Regions where the impact intensity of Ts on SIF (R(SIF, Ts|SM)) was more than SM (R(SIF,SM|Ts)) were widespread, especially along the latitudinal gradient (Figure 6e, f). Overall, 71.86% of the terrestrial vegetation areas showed above 0 values in R(SIF, Ts|SM)-R(SIF,SM|Ts), mainly distributed in middle and high latitudes and South America. In comparison, 28.14% of the terrestrial vegetation areas showed below 0 values in R(SIF, Ts|SM)-R(SIF,SM|Ts), mainly distributed in the middle and low latitudes (Africa, India, Australia, and some regions of South America). Moreover, areas with |R(SIF, Ts|SM)|-|R(SIF,SM|Ts)| greater than 0 accounted for 64.17%, indicating that in almost two-thirds of areas, Ts is more correlated with SIF than SM. Meanwhile, the spatial distribution of SIF we obtained is consistent with the one from GOME-2 SIF data (Figure S13). In addition, the spatial distribution of the partial correlation between SIF and Ts, SM_{root} was highly consistent with those between SIF and Ts, surface SM (Figure 6 and Figure S16). The results from the partial correlation analysis indicated that Ts played a more important role than SM for vegetation productivity at the global scale. The analysis using SM-Ts bins decoupling also confirms the validity of this claim.

3.4 | Sensitivity of Ts and SM on climate and vegetation gradient

In this study, we found that the promotion by SA_{Ts} ($\Delta SA_{SIF}(SA_{Ts}|SA_{SM})$) was the greatest in humid ecosystems ($\Delta SA_{SIF}(SA_{Ts}|SA_{SM})$ = 1.0

Partial correlation	Positive	Positive $p < .05$	Negative	Negative $p < .05$
R(SIF, Ts|SM)	89.70%	87.56%	10.30%	10.30%
R(SIF,SM|Ts)	54.23%	51.68%	45.77%	45.77%
R(SIF, Ts|SM)-R(SIF,SM|Ts)	71.86%	–	28.14%	–
R(SIF, Ts|SM_{root})	91.34%	86.73%	8.66%	4.90%
R(SIF,SM_{root}|Ts)	55.74%	48.56%	44.26%	31.77%
R(SIF, Ts|SM_{root})-R(SIF,SM_{root}|Ts)	73.12%	–	26.88%	–

TABLE 1 Partial correlations between SIF and Ts, surface SM (referred to as SM) and root SM (SM_{root}), respectively

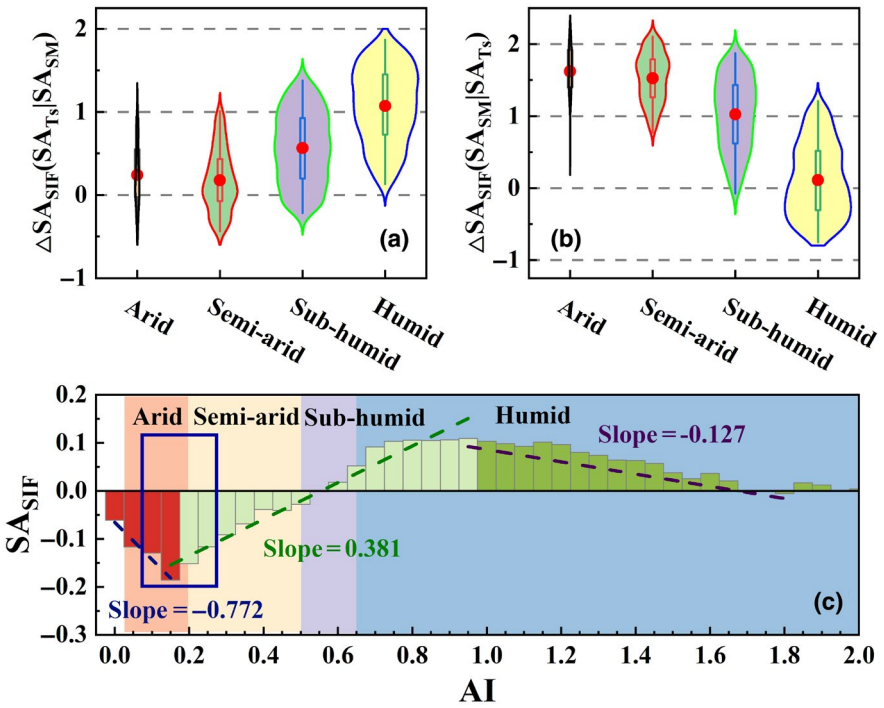

FIGURE 7 Sensitivity of Ts and SM to the gradient of climate and vegetation gradients. (a) Violin plot of Ts ($\triangle SA_{SIF}(SA_{Ts}|SA_{SM})$) effects on the aridity gradient. (b) Violin plot of SM ($\triangle SA_{SIF}(SA_{SM}|SA_{Ts})$) effects across an aridity gradient. (c) Sensitivity of SIF under different climatic conditions. The dashed lines indicate the linear regressions of SIF standardized anomaly versus aridity values, and the Slope values represent the regression coefficients of SIF standardized anomaly with aridity index (AI) [Colour figure can be viewed at wileyonlinelibrary.com]

74 ± 0.456) and the smallest in semi-arid ecosystems ($\Delta SA_{SIF}(SA_{Ts}|SA_{SM})$ = 0.176 ± 0.367) (Figure 7a), e.g., scrub, grassland, and savanna ecosystems. Comparatively, the facilitation effect of SA_{SM} ($\Delta SA_{SIF}(SA_{SM}|SA_{Ts})$) was apparent in arid ($\Delta SA_{SIF}(SA_{SM}|SA_{Ts})$ = 1.620 ± 0.369), semi-arid ($\Delta SA_{SIF}(SA_{SM}|SA_{Ts})$ = 1.528 ± 0.337) ecosystems, and the facilitation effect in humid ecosystems ($\Delta SA_{SIF}(SA_{SM}|SA_{Ts})$ = 0.111 ± 0.507) was trivial (Figure 7b). Semi-arid ecosystems were major drivers of global terrestrial CO_2 flux changes (Ahlstrom et al., 2015; Poulter et al., 2014). The increases in SM are believed to have a higher impact on vegetation productivity in arid and semi-arid regions than Ts. In addition, as SM is experiencing a decreasing trend globally (Deng et al., 2020), and the dryland area is predicted to be expanding (Huang et al., 2015), the impact of SM on the global carbon cycle is expected to increase in the future. In addition, deforestation and degradation of tropical rainforests were important drivers of global CO_2 flux changes in terrestrial ecosystems (Qin et al., 2021). The results of our study showed that in the humid zone, the variation of Ts played a more important role in vegetation productivity, but in the arid and semi-arid zones, the variation of SM played a more important role in vegetation productivity; in the semi-humid zone, the disparity in the importance of SM and Ts is difficult to unravel.

The role of drought stress on vegetation photosynthetic CO_2 assimilation was considered as one of the largest uncertainties in predicting future land carbon uptake and climate change (Hagemann et al., 2013; Prudhomme et al., 2014). However, empirical functions (usually not validated against observed empirical data) that depend only on plant functional types were usually in terrestrial ecosystem models to capture drought stress (Dai et al., 2003). In this study, we explored the sensitivity of SA_{SIF} to AI. The aridity sensitivity of SA_{SIF} showed inconsistent patterns with climate gradient. The sensitivity of SA_{SIF} to AI fluctuated, with increased climate wetness, peaking in arid and semi-arid zones (Figure 7c), which was similar to the finding by Liu et al. (2018). Therefore, we believe the results of this study are able to provide suggestions for the improvement of terrestrial ecosystem models.

4 | CONCLUSIONS

Taking advantage of SIF, Ts, and SM data from 2000 to 2020, we decoupled the joint impact of Ts and SM on global ecosystem productivity using bin decoupling and partial correlation analysis. The results indicated that Ts contributed more to ecosystem productivity than SM in global vegetation-covered regions. However, the importance of SM and Ts varied, given different vegetation types. The results showed that in the humid zone, the variation of Ts played a more important role in vegetation productivity, but in the arid and semi-arid zones, the variation of SM played a more important role; in the semi-humid zone, their relative importance is difficult to unravel. We thus argue the necessity of re-evaluating whether a warming climate can further promote vegetation growth by considering the different roles of Ts and SM on different vegetation types. The results of this study can be implemented into the terrestrial ecosystem model to better predict vegetation productivity at regional and global scales, reducing uncertainty in the assessment of CO_2 uptake from terrestrial vegetation and providing more insight into the response of vegetation to climate change.

ACKNOWLEDGMENTS

This work was supported in part by the National Key R&D Program of China under Grant 2018YFB2100501; in part by the National Natural Science Foundation of China under Grants 42090012, 41771452, 41771454; 03 Special Research and 5G Project of Jiangxi Province in China under Grant 20212ABC03A09; Zhuhai Industry University Research Cooperation Project of China under Grant ZH22017001210098PWC.

CONFLICT OF INTEREST

The authors declare no competing interests.

DATA AVAILABILITY STATEMENT

GOSIF data are available at http://data.globalecology.unh.edu/data/GOSIF_v2/; GOME-2 SIF data are available at https://avdc.gsfc.nasa.gov/pub/data/satel lite/MetOp/ GOME_F/v28/; CRU climatic data are available at http://www.cru.uea.ac.uk/data/; GLEAM data are available at https://www.gleam.eu; MODIS Land Cover Type data are available at https://e4ftl01.cr.usgs.gov/MODV6_Cmp_C/MOTA/MCD12C1.006/; GLASS data are available at http://www.glass.umd.edu/GPP/AVHRR/.

ORCID

Chaoya Dang https://orcid.org/0000-0001-7141-2270

REFERENCES

Ahlstrom, A., Raupach, M. R., Schurgers, G., Smith, B., Arneth, A., Jung, M., Reichstein, M., Canadell, J. G., Friedlingstein, P., Jain, A. K., Kato, E., Poulter, B., Sitch, S., Stocker, B. D., Viovy, N., Wang, Y. P., Wiltshire, A., Zaehle, S., & Zeng, N. (2015). The dominant role of semi-arid ecosystems in the trend and variability of the land CO_2 sink. *Science*, *348*(6237), 895–899. https://doi.org/10.1126/science.aaa1668

Albergel, C., Dorigo, W., Reichle, R. H., Balsamo, G., de Rosnay, P., Muñoz-Sabater, J., Isaksen, L., de Jeu, R., & Wagner, W. (2013). Skill and global trend analysis of soil moisture from reanalyses and microwave remote sensing. *Journal of Hydrometeorology*, *14*(4), 1259–1277. https://doi.org/10.1175/JHM-D-12-0161.1

Beck, H. E., Pan, M., Miralles, D. G., Reichle, R. H., Dorigo, W. A., Hahn, S., Sheffield, J., Karthikeyan, L., Balsamo, G., Parinussa, R. M., van Dijk, A. I. J. M., Du, J., Kimball, J. S., Vergopolan, N., & Wood, E. F. (2021). Evaluation of 18 satellite- and model-based soil moisture products using in situ measurements from 826 sensors. *Hydrology and Earth System Sciences*, *25*(1), 17–40. https://doi.org/10.5194/hess-25-17-2021

Burgin, M. S., Colliander, A., Njoku, E. G., Chan, S. K., Cabot, F., Kerr, Y. H., Bindlish, R., Jackson, T. J., Entekhabi, D., & Yueh, S. H. (2017). A comparative study of the SMAP passive soil moisture product with existing satellite-based soil moisture products. *IEEE Transactions on Geoscience and Remote Sensing*, *55*(5), 2959–2971. https://doi.org/10.1109/TGRS.2017.2656859

Chen, X. J., Mo, X. G., Zhang, Y. C., Sun, Z. G., Liu, Y., Hu, S., & Liu, S. X. (2019). Drought detection and assessment with solar-induced

chlorophyll fluorescence in summer maize growth period over North China Plain. *Ecological Indicators*, *104*, 347–356. https://doi.org/10.1016/j.ecolind.2019.05.017

Christopher, B. F., James, T. R., & Carolyn, M. M. (1995). Global net primary production: Combining ecology and remote sensing. *Remote Sensing of Environment*, *51*(1), 74–88. https://doi.org/10.1016/0034-4257(94)00066-v

Craig, D. A., Alison, K. M., Haroun, C., Dominique, B., Nate, M., Michel, V., Thomas, K., Andreas, R., David, D. B., Hogg, E. H., Patrick, G., Rod, F., Zhen, Z., Jorge, C., Natalia, D., Jong-Hwan, L., Gillian, A., Steven, W. R., Akkin, S., & Neil, C. (2010). A global overview of drought and heat-induced tree mortality reveals emerging climate change risks for forests. *Forest Ecology and Management*, *259*(4), 660–684. https://doi.org/https://doi.org/10.1016/j.foreco.2009.09.001

Dai, Y. J., Zeng, X. B., Dickinson, R. E., Baker, I., Bonan, G. B., Bosilovich, M. G., Denning, A. S., Dirmeyer, P. A., Houser, P. R., Niu, G. Y., Oleson, K. W., Schlosser, C. A., & Yang, Z. L. (2003). The Common Land Model. *Bulletin of the American Meteorological Society*, *84*(8), 1013–1023. https://doi.org/10.1175/BAMS-84-8-1013

Deng, Y. H., Wang, S. J., Bai, X. Y., Luo, G. J., Wu, L. H., Cao, Y., Li, H. W., Li, C. J., Yang, Y. J., Hu, Z. Y., & Tian, S. Q. (2020). Variation trend of global soil moisture and its cause analysis. *Ecological Indicators*, *110*, 105939. https://doi.org/10.1016/j.ecolind.2019.105939

Feng, S., & Fu, Q. (2013). Expansion of global drylands under a warming climate. *Atmospheric Chemistry and Physics*, *13*(19), 10081–10094. https://doi.org/10.5194/acp-13-10081-2013

Frankenberg, C., Fisher, J. B., Worden, J., Badgley, G., Saatchi, S. S., Lee, J., Toon, G. C., Butz, A., Jung, M., Kuze, A., & Yokota, T. (2011). New global observations of the terrestrial carbon cycle from GOSAT: Patterns of plant fluorescence with gross primary productivity. *Geophysical Research Letters*, *38*(17), 706. https://doi.org/10.1029/2011gl048738

Green, J. K., Seneviratne, S. I., Berg, A. M., Findell, K. L., Hagemann, S., Lawrence, D. M., & Gentine, P. (2019). Large influence of soil moisture on long-term terrestrial carbon uptake. *Nature*, *565*(7740), 476–479. https://doi.org/10.1038/s41586-018-0848-x

Guanter, L., Zhang, Y., Jung, M., Joiner, J., Voigt, M., Berry, J. A., Frankenberg, C., Huete, A. R., Zarco-Tejada, P., Lee, J.-E., Moran, M. S., Ponce-Campos, G., Beer, C., Camps-Valls, G., Buchmann, N., Gianelle, D., Klumpp, K., Cescatti, A., Baker, J. M., & Griffis, T. J. (2014). Global and time-resolved monitoring of crop photosynthesis with chlorophyll fluorescence. *Proceedings of the National Academy of Sciences of the United States of America*, *111*(14), E1327–E1333. https://doi.org/10.1073/pnas.1320008111

Hagemann, S., Chen, C., Clark, D. B., Folwell, S., Gosling, S. N., Haddeland, I., Hanasaki, N., Heinke, J., Ludwig, F., Voss, F., & Wiltshire, A. J. (2013). Climate change impact on available water resources obtained using multiple global climate and hydrology models. *Earth System Dynamics*, *4*(1), 129–144. https://doi.org/10.5194/esd-4-129-2013

Harris, I., Osborn, T. J., Jones, P., & Lister, D. (2020). Version 4 of the CRU TS monthly high-resolution gridded multivariate climate dataset. *Scientific Data*, *7*(1), 109. https://doi.org/10.1038/s41597-020-0453-3

Huang, J. P., Yu, H. P., Guan, X. D., Wang, G. Y., & Guo, R. X. (2015). Accelerated dryland expansion under climate change. *Nature Climate Change*, *6*, 166–171. https://doi.org/10.1038/nclimate2837

Huang, M. T., Piao, S. L., Ciais, P., Peñuelas, J., Wang, X. H., Keenan, T. F., Peng, S. S., Berry, J. A., Wang, K., Mao, J. F., Alkama, R., Cescatti, A., Cuntz, M., Hannes, D. D., Gao, M. D., He, Y., Liu, Y. W., Luo, Y. Q., Myneni, R. B., … Janssens, I. A. (2019). Air temperature optima of vegetation productivity across global biomes. *Nature Ecology & Evolution*, *3*(5), 772–779. https://doi.org/10.1038/s41559-019-0838-x

Humphrey, V., Berg, A., Ciais, P., Gentine, P., Jung, M., Reichstein, M., Seneviratne, S. I., & Frankenberg, C. (2021). Soil moisture–atmosphere feedback dominates land carbon uptake variability. *Nature*, *592*(7852), 65–69. https://doi.org/10.1038/s41586-021-03325-5

Humphrey, V., Zscheischler, J., Ciais, P., Gudmundsson, L., Sitch, S., & Seneviratne, S. I. (2018). Sensitivity of atmospheric CO_2 growth rate to observed changes in terrestrial water storage. *Nature*, *560*(7720), 628–631. https://doi.org/10.1038/s41586-018-0424-4

Joiner, J., Guanter, L., Lindstrot, R., Voigt, M., Vasilkov, A. P., Middleton, E. M., Huemmrich, K. F., Yoshida, Y., & Frankenberg, C. (2013). Global monitoring of terrestrial chlorophyll fluorescence from moderate spectral resolution near-infrared satellite measurements: Methodology, simulations, and application to GOME-2. *Atmospheric Measurement Techique Discussion*, *6*(2), 3883–3930. https://doi.org/10.5194/amtd-6-3883-2013

Köhler, P., Guanter, L., & Joiner, J. (2014). A linear method for the retrieval of sun-induced chlorophyll fluorescence from GOME-2 and SCIAMACHY data. *Atmospheric Measurement Techique Discussion*, *7*(12), 12173–12217. https://doi.org/10.5194/amtd-7-12173-2014

Koster, R. D., Dirmeyer, P. A., Guo, Z., Bonan, G., Chan, E., Cox, P., Gordon, C. T., Kanae, S., Kowalczyk, E., Lawrence, D., Liu, P., Lu, C.-H., Malyshev, S., McAvaney, B., Mitchell, K., Mocko, D., Oki, T., Oleson, K., Pitman, A., … Yamada, T. (2004). Regions of strong coupling between soil moisture and precipitation. *Science*, *305*(5687), 1138–1140. https://doi.org/10.1126/science.1100217

Koster, R. D., Sud, Y. C., Guo, Z. C., Dirmeyer, P. A., Bonan, G., Oleson, K. W., Chan, E., Verseghy, D., Cox, P., Davies, H., Kowalczyk, E., Gordon, C. T., Kanae, S., Lawrence, D., Liu, P., Mocko, D., Lu, C. H., Mitchell, K., Malyshev, S., … Xue, Y. K. (2006). GLACE: The Global Land-Atmosphere Coupling Experiment. Part I: Overview. *Journal of Hydrometeorology*, *7*(4), 590–610. https://doi.org/10.1175/JHM510.1

Li, X., & Xiao, J. F. (2019a). A global, 0.05-Degree product of solar-induced chlorophyll fluorescence derived from OCO-2, MODIS, and reanalysis data. *Remote Sensing*, *11*(5), 517. https://doi.org/10.3390/rs11050517

Li, X., & Xiao, J. F. (2019b). Mapping photosynthesis solely from solar-induced chlorophyll fluorescence: A global, fine-resolution dataset of gross primary production derived from OCO-2. *Remote Sensing*, *11*(21), 2563. https://doi.org/10.3390/rs11212563

Li, X., Xiao, J. F., He, B. B., Arain, M. A., Beringer, J., Desai, A. R., Emmel, C., Hollinger, D. Y., Krasnova, A., Mammarella, I., Noe, S. M., Penélope, S. O., Rey-Sanchez, C., Rocha, A. V., & Varlagin, A. (2018). Solar-induced chlorophyll fluorescence is strongly correlated with terrestrial photosynthesis for a wide variety of biomes: First global analysis based on OCO-2 and flux tower observations. *Global Change Biology*, *24*(9), 3990–4008. https://doi.org/10.1111/gcb.14297

Liang, S., Cheng, C., Jia, K., Jiang, B., Liu, Q., Xiao, Z., Yao, Y., Yuan, W., Zhang, X., Zhao, X., & Zhou, J. (2020). The Global LAnd Surface Satellite (GLASS) products suite. *Bulletin of the American Meteorological Society*, E323–E337. https://doi.org/10.1175/BAMS-D-1118-0341.1171

Liu, J. J., Wennberg, P. O., Parazoo, N. C., Yin, Y., & Frankenberg, C. (2020). Observational constraints on the response of high-latitude northern forests to warming. *AGU Advances*, *1*(4), e2020av000228. https://doi.org/10.1029/2020av000228

Liu, L., Gudmundsson, L., Hauser, M., Qin, D., Li, S., & Seneviratne, S. I. (2020). Soil moisture dominates dryness stress on ecosystem production globally. *Nature Communications*, *11*(1), 4892. https://doi.org/10.1038/s41467-020-18631-1

Liu, L. B., Peng, S. S., AghaKouchak, A., Huang, Y. Y., Li, Y., Qin, D. H., Xie, A. L., & Li, S. C. (2018). Broad consistency between satellite and vegetation model estimates of Net Primary Productivity

across global and regional scales. *Journal of Geophysical Research: Biogeosciences*, https://doi.org/10.1029/2018jg004760

Liu, Y., Dang, C. Y., Yue, H., Lyu, C. G., & Dang, X. H. (2021). Enhanced drought detection and monitoring using sun-induced chlorophyll fluorescence over Hulun Buir Grassland, China. *Science of the Total Environment*, *770*, https://doi.org/10.1016/j.scitotenv.2021.145271

Madadgar, S., AghaKouchak, A., Farahmand, A., & Davis, S. J. (2017). Probabilistic estimates of drought impacts on agricultural production. *Geophysical Research Letters*, *44*(15), 7799–7807. https://doi.org/10.1002/2017GL073606

Martens, B., Miralles, D., Lievens, H., Fernández-Prieto, D., & Verhoest, N. E. C. (2015). Improving terrestrial evaporation estimates over continental Australia through assimilation of SMOS soil moisture. *International Journal of Applied Earth Observation and Geoinformation*, *S0303243415300350*, https://doi.org/10.1016/j.jag.2015.09.012

Martens, B., Miralles, D. G., Lievens, H., van der Schalie, R., de Jeu, R. A. M., Fernández-Prieto, D., Beck, H. E., Dorigo, W. A., & Verhoest, N. E. C. (2017). GLEAM v3: Satellite-based land evaporation and root-zone soil moisture. *Geoscientific Model Development*, *10*(5), 1903–1925. https://doi.org/10.5194/gmd-10-1903-2017

Medlyn, B. E., Dreyer, E., Ellsworth, D., Forstreuter, M., Harley, P. C., Kirschbaum, M. U. F., Le Roux, X., Montpied, P., Strassemeyer, J., Walcroft, A., Wang, K., & Loustau, D. (2002). Temperature response of parameters of a biochemically based model of photosynthesis. II. A review of experimental data. *Plant, Cell & Environment*, *25*(9), 1167–1179. https://doi.org/10.1046/j.1365-3040.2002.00891.x

Miralles, D. G., Holmes, T. R. H., De Jeu, R. A. M., Gash, J. H., Meesters, A. G. C. A., & Dolman, A. J. (2011). Global land-surface evaporation estimated from satellite-based observations. *Hydrology and Earth System Sciences*, *15*(2), 453–469. https://doi.org/10.5194/hess-15-453-2011

Nemani, R. R. (2003). Climate-driven increases in global terrestrial net primary production from 1982 to 1999. *Science*, *300*, 1560–1563. https://doi.org/10.2307/3834473

Nistor, M. M. (2019). Vulnerability of groundwater resources under climate change in the Pannonian basin. *Geo-spatial Information Science*, *22*(4), 345–438. https://doi.org/10.1080/10095020.2019.1613776

Niu, S. L., Li, Z. X., Xia, J. Y., Han, Y., Wu, M. I., & Wan, S. Q. (2008). Climatic warming changes plant photosynthesis and its temperature dependence in a temperate steppe of northern China. *Environmental and Experimental Botany*, *63*(1–3), 91–101. https://doi.org/10.1016/j.envexpbot.2007.10.016

Padilla, F. M., & Pugnaire, F. I. (2007). Rooting depth and soil moisture control Mediterranean woody seedling survival during drought. *Functional Ecology*, *21*(3), 489–495. https://doi.org/10.2307/4540047

Park, W. A., Allen, C. D., Macalady, A. K., Griffin, D., Woodhouse, C. A., Meko, D. M., Swetnam, T. W., Rauscher, S. A., Seager, R., Grissino-Mayer, H. D., Dean, J. S., Cook, E. R., Gangodagamage, C., Cai, M., & McDowell, N. G. (2012). Temperature as a potent driver of regional forest drought stress and tree mortality. *Nature Climate Change*, *3*(3), 292–297. https://doi.org/10.1038/nclimate1693

Porcar-Castell, A., Tyystjarvi, E., Atherton, J., van der Tol, C., Flexas, J., Pfundel, E. E., Moreno, J., Frankenberg, C., & Berry, J. A. (2014). Linking chlorophyll a fluorescence to photosynthesis for remote sensing applications: Mechanisms and challenges. *Journal of Experimental Botany*, *65*(15), 4065–4095. https://doi.org/10.1093/jxb/eru191

Poulter, B., Frank, D., Ciais, P., Myneni, R. B., Andela, N., Bi, J., Broquet, G., Canadell, J. G., Chevallier, F., Liu, Y. Y., Running, S. W., Sitch, S., & van der Werf, G. R. (2014). Contribution of semi-arid ecosystems to interannual variability of the global carbon cycle. *Nature*, *509*(7502), 600–603. https://doi.org/10.1038/nature13376

Prudhomme, C., Giuntoli, I., Robinson, E. L., Clark, D. B., Arnell, N. W., Dankers, R., Fekete, B. M., Franssen, W., Gerten, D., Gosling, S. N., Hagemann, S., Hannah, D. M., Kim, H., Masaki, Y., Satoh, Y., Stacke, T., Wada, Y., & Wisser, D. (2014). Hydrological droughts in the 21st century, hotspots and uncertainties from a global multimodel ensemble experiment. *Proceedings of the National Academy of Sciences of the United States of America*, *111*(9), 3262–3267. https://doi.org/10.1073/pnas.1222473110

Qin, Y., Xiao, X., Wigneron, J.-P., Ciais, P., Brandt, M., Fan, L., Li, X., Crowell, S., Wu, X., Doughty, R., Zhang, Y., Liu, F., Sitch, S., & Moore, B. (2021). Carbon loss from forest degradation exceeds that from deforestation in the Brazilian Amazon. *Nature Climate Change*, *11*, 442–448. https://doi.org/10.1038/s41558-021-01026-5

Rogers, A., Medlyn, B. E., Dukes, J. S., Bonan, G., von Caemmerer, S., Dietze, M. C., Kattge, J., Leakey, A. D. B., Mercado, L. M., Niinemets, Ü., Prentice, I. C., Serbin, S. P., Sitch, S., Way, D. A., & Zaehle, S. (2017). A roadmap for improving the representation of photosynthesis in Earth system models. *New Phytologist*, *213*(1), 22–42. https://doi.org/10.1111/nph.14283

Sage, R. F., & Kubien, D. S. (2007). The temperature response of C_3 and C_4 photosynthesis. *Plant, Cell and Environment*, *30*(9), 1086–1106. https://doi.org/10.1111/j.1365-3040.2007.01682.x

Seneviratne, S. I., Corti, T., Davin, E. L., Hirschi, M., Jaeger, E. B., Lehner, I., Orlowsky, B., & Teuling, A. J. (2010). Investigating soil moisture–climate interactions in a changing climate: a review. *Earth Science Reviews*, *99*(3–4), 125–161. https://doi.org/10.1016/j.earscirev.2010.02.004

Seneviratne, S. I., & Stöckli, R. (2007). The role of land–atmosphere interactions for climate variability in Europe. In S. Bronnimann, J. Luterbacher, T. Ewen, H. F. Diaz, R. S. Stolarski, & U. Neu (Eds.), *Climate variability and extremes during the past 100 years. Book Series: Advances in global change research* (vol. 33, pp. 179–193). Springer.

Shao, Z. F., Li, C. M., Li, D. R., Altan, O., Zhang, L., & Ding, L. (2020). An accurate matching method for projecting vector data into surveillance video to monitor and protect cultivated land. *ISPRS International Journal of Geo-Information*, *9*(7), 448. https://doi.org/10.3390/ijgi9070448

Sonia, I. S., Thierry, C., Edouard, L. D., Martin, H., Eric, B. J., Irene, L., Boris, O., & Adriaan, J. T. (2010). Investigating soil moisture–climate interactions in a changing climate: A review. *Earth Science Reviews*, *99*(3–4), 125–161. https://doi.org/10.1016/j.earscirev.2010.02.004

Stocker, T., Plattner, G. K., & Dahe, Q. (Eds). (2013). *IPCC Climate Change 2013: The Physical Science Basis*. Cambridge University Press.

Stocker, B. D., Zscheischler, J., Keenan, T. F., Prentice, I. C., Peñuelas, J., & Seneviratne, S. I. (2018). Quantifying soil moisture impacts on light use efficiency across biomes. *New Phytologist*, *218*(4), 1430–1449. https://doi.org/10.1111/nph.15123

Sun, Y., Fu, R., Dickinson, R., Joiner, J., Frankenberg, C., Gu, L. H., Xia, Y. Y., & Fernando, N. (2015). Drought onset mechanisms revealed by satellite solar-induced chlorophyll fluorescence: Insights from two contrasting extreme events. *Journal of Geophysical Research: Biogeosciences*, *120*(11), 2427–2440. https://doi.org/10.1002/2015JG003150

Taylor, C. M., de Jeu, R. A. M., Guichard, F., Harris, P. P., & Dorigo, W. A. (2012). Afternoon rain more likely over drier soils. *Nature*, *489*(7416), 423–426. https://doi.org/10.1038/nature11377

Walther, S., Duveiller, G., Jung, M., Guanter, L., Cescatti, A., & Camps-Valls, G. (2019). Satellite observations of the contrasting response of trees and grasses to variations in water availability. *Geophysical Research Letters*, *46*(3), 1429–1440. https://doi.org/10.1029/2018gl080535

Wang, X. R., Qiu, B., Li, W. K., & Zhang, Q. (2019). Impacts of drought and heatwave on the terrestrial ecosystem in China as revealed by satellite solar-induced chlorophyll fluorescence. *Science of the Total Environment*, *693*, 133627. https://doi.org/10.1016/j.scitotenv.2019.133627.

Williams, L. E., Baeza, P., & Vaughn, P. (2012). Midday measurements of leaf water potential and stomatal conductance are highly correlated with daily water use of thompson seedless grapevines.

Irrigation Science, *30*(3), 201–212. https://doi.org/10.1007/s00271-011-0276-2

Xu, C., McDowell, N. G., Fisher, R. A., Wei, L., Sevanto, S., Christoffersen, B. O., Weng, E., & Middleton, R. S. (2019). Increasing impacts of extreme droughts on vegetation productivity under climate change. *Nature Climate Change*, *9*(12), 948–953. https://doi.org/10.1038/s41558-019-0630-6

Yao, J. Y., Liu, H. P., Huang, J. P., Gao, Z. M., Wang, G. Y., Li, D., Yu, H. P., & Chen, X. Y. (2020). Accelerated dryland expansion regulates future variability in dryland gross primary production. *Nature Communications*, *11*(1), 1665. https://doi.org/10.1038/s41467-020-15515-2

Yoshida, Y., Joiner, J., Tucker, C., Berry, J., Lee, J.-E., Walker, G., Reichle, R., Koster, R., Lyapustin, A., & Wang, Y. (2015). The 2010 Russian drought impact on satellite measurements of solar-induced chlorophyll fluorescence: Insights from modeling and comparisons with parameters derived from satellite reflectances. *Remote Sensing of Environment*, *166*, 163–177. https://doi.org/10.1016/j.rse.2015.06.008

Zhang, Y., & Shao, Z. F. (2021). Assessing of urban vegetation biomass in combination with LiDAR and high-resolution remote sensing images. *International Journal of Remote Sensing*, *42*(3), 964–985. https://doi.org/10.1080/01431161.2020.1820618

SUPPORTING INFORMATION

Additional supporting information may be found in the online version of the article at the publisher's website.

How to cite this article: Dang, C., Shao, Z., Huang, X., Qian, J., Cheng, G., Ding, Q., & Fan, Y. (2022). Assessment of the importance of increasing temperature and decreasing soil moisture on global ecosystem productivity using solar-induced chlorophyll fluorescence. *Global Change Biology*, 28, 2066–2080. https://doi.org/10.1111/gcb.16043